Antarctic bottom and lower circumpolar deep water circulation in the eastern Indian Ocean

Bernadette M. Sloyan[1,2]

Received 19 April 2005; revised 1 September 2005; accepted 14 November 2005; published 15 February 2006.

[1] Net northward transport below $\gamma^n > 28.1$ kg m^{-3} ($\approx$3200 m) into the Perth Basin of between 4.4 and 5.8 Sv is estimated from a year-long current meter mooring array between the Broken and Naturaliste plateaus. Northward transport of between 2.0 and 2.5 Sv of Antarctic Bottom Water ($\gamma^n > 28.2$ kg m^{-3}), that must upwell within the southern region of the Perth Basin, results in an area-averaged diapycnal velocity and diffusivity of $w^* = 2.5–3.1 \times 10^{-6}$ m s^{-1} and $\kappa = 13–15 \times 10^{-4}$ m^2 s^{-1}, respectively. Diffusivity estimates for the Perth Basin are several times larger than area-averaged mixing estimates for the abyssal subtropical South Atlantic and Pacific oceans. However, the dissipation of turbulent kinetic energy required to maintain the abyssal mixing in the Perth Basin, $\epsilon = O(10^{-9}$ W kg$^{-1})$, is similar to that required in the South Atlantic Ocean. The area-averaged diffusivity in the Perth Basin does not require unreasonable energy dissipation rates as this ocean basin is only weakly stratified. The abyssal diffusivity of the Perth Basin results from intense mixing at the basin boundary and in the basin interior over rough topography. The complex bathymetry and low abyssal stratification suggests that the Indian Ocean, for a given energy dissipation, may support a larger meridional overturning circulation than other subtropical basins.

Citation: Sloyan, B. M. (2006), Antarctic bottom and lower circumpolar deep water circulation in the eastern Indian Ocean, *J. Geophys. Res.*, *111*, C02006, doi:10.1029/2005JC003011.

1. Introduction

[2] Antarctic Bottom Water (AABW) formation appears to be concentrated on the continental margins where mixing between deep water and shelf water occurs [*Jacobs*, 1986]. Principal sites of AABW production include the Weddell Sea, Ross Sea and along Adélie Coast [*Sverdrup et al.*, 1942; *Carmack*, 1977; *Gordon and Tchernia*, 1972; *Baines and Condie*, 1998; *Park et al.*, 1998; *Rintoul*, 1998; *Orsi et al.*, 1999; *Whitworth*, 2002]. AABW subsequently flows northward into the three abyssal basins of the Southern Ocean: Weddell-Enderby Basin, Australian-Antarctic Basin, and Southeast Pacific Basin. As AABW is transported northward off the continental slope and circulates in the abyssal gyres, it mixes with the overlying water producing the slightly less dense Lower Circumpolar Deep Water (LCDW). AABW and LCDW spread northward to fill the deep Atlantic, Indian, and Pacific basins [*Sloyan and Rintoul*, 2001]. The northward flow of AABW and LCDW must upwell in the subtropical oceans and return to the Southern Ocean to close the meridional overturning circulation.

[3] In the Indian Ocean, observational-based estimates of deep northward transport of AABW and LCDW across 32°S vary widely between 10 Sv (1 Sv = 1×10^6 m^3 s^{-1}) and 25 Sv [*Toole and Warren*, 1993; *Schmitz*, 1996; *Robbins and Toole*, 1997; *Macdonald*, 1998; *Ganachaud et al.*, 2000; *Sloyan and Rintoul*, 2001; *Bryden and Beal*, 2001; *Talley et al.*, 2003]. Property distributions on potential–density anomaly surfaces show that bathymetric features constrain the spreading path of AABW and LCDW into the Indian Ocean abyssal basins [*Mantyla and Reid*, 1995]. The effect of topography is to guide (restrict) the transport of AABW and LCDW into the deep western boundary currents of the Natal, Mozambique, Madagascar, Crozet and Perth basins [*Warren*, 1981; *Toole and Warren*, 1993; *Mantyla and Reid*, 1995].

[4] The bottom and deep waters in the eastern Indian Ocean are derived from AABW originating in the Ross Sea and along the Adélie coast [*Mantyla and Reid*, 1995], entering the region via the Australian-Antarctic and South Australian basins [*Hufford et al.*, 1997; *Donohue et al.*, 1999] (also M. S. McCartney and K. A. Donohue, A deep cyclonic gyre in the Australian-Antarctic Basin, submitted to *Progress in Oceanography*, 2005). AABW and LCDW fill the abyssal basins of the Perth and West Australian basins, and spill into the Central Indian Basin through numerous deep sills in the Ninetyeast Ridge [*Warren*, 1981, 1982; *Toole and Warren*, 1993; *Mantyla and Reid*, 1995; *McCarthy et al.*, 1997; *Talley and Baringer*, 1997; *Warren and Johnson*, 2002]. Overlying the northward transport of AABW and LCDW is a southward return

[1]Woods Hole Oceanographic Institution, Woods Hole, Massachusetts, USA.
[2]Now at CSIRO Marine and Atmospheric Research, Hobart, Tasmania, Australia.

0148-0227/06/2005JC003011$09.00

flow (between 2000 and 4000 m) of oxygen poor and enhanced nutrient water: Indian Deep Water [*Toole and Warren*, 1993].

[5] Estimates of the northward transport of AABW and LCDW into the eastern Indian Ocean at 32°S are derived from the thermal wind shear with a deep (3500–4000 m) zero-velocity surface chosen on the basis of property distributions [*Toole and Warren*, 1993; *Schmitz*, 1996; *Robbins and Toole*, 1997; *Talley and Baringer*, 1997; *Macdonald*, 1998; *Ganachaud et al.*, 2000; *Sloyan and Rintoul*, 2001]. In the Perth Basin, *Toole and Warren* [1993] estimate a net northward deep water transport of 6.1 Sv (below 2000 m) which consists of 7.1 Sv northward transport in the western boundary current at the Broken Plateau (101°E–108°E) and southward transport of 1 Sv between 108°E and 110°E, while *Talley and Baringer* [1997] estimate a net northward transport of 5.2 Sv (6.6 Sv boundary current and 1.4 Sv southward). Inverse studies of *Ganachaud et al.* [2000] and *Sloyan and Rintoul* [2001] estimate a net northward transport of deep water (below ≈2000 m) into the Perth Basin of 1 ± 8 Sv, and 7 ± 2 Sv (8.3 ± 2 Sv boundary current, and 1.3 ± 1 Sv interior southward), respectively. (*Robbins and Toole* [1997] constrain the deep transport into the Perth Basin based on the *Toole and Warren* [1993] deep transport estimates.) Indian Ocean area-averaged diapycnal velocity and diffusivity vary between 3×10^{-7} m s^{-1} and 6×10^{-6}m s^{-1}, and $2–10 \times 10^{-4}$ m^{2}s^{-1}, respectively [*Warren*, 1981; *Toole and Warren*, 1993; *Robbins and Toole*, 1997; *Macdonald*, 1998; *Ganachaud et al.*, 2000; *Sloyan and Rintoul*, 2001]. These studies consistently suggest that mixing rates in the Indian Ocean are several times larger than mixing rates in the Pacific and South Atlantic oceans.

[6] The present study examines the abyssal circulation of the eastern Indian Ocean. We provide direct estimates of the absolute bottom and deep water (below 3200 m) transport into the Perth Basin, and abyssal mixing determined from a 1-year current meter mooring array that was deployed between the Broken and Naturaliste plateaus and numerous hydrographic surveys. Details of the mooring array, and data processing are discussed in section 2. Section 3 discusses the quasi-synoptic and mean vector velocity and transport into the Perth Basin. The implied mixing (section 4) and dissipation of kinetic energy (section 5) estimates are compared with similar estimates for the Somali Basin (eastern Indian Ocean), Brazil Basin (South Atlantic) and Scotia Sea to provide a perspective of the strength of Indian Ocean abyssal mixing. The discussion and conclusions (section 6) close the paper.

2. Current Meter Mooring Array and Hydrographic Data

[7] Ten current meter moorings were deployed between the Broken and Naturaliste plateaus in June–July 1995 (Figure 1). Nine moorings were recovered in September 1996 (Figure 2). Aanderaa RCM8 current meters were principally used in the recovered array (20 of 25), while the remaining current meters were Aanderaa RCM5. Data were recovered from all instruments, although the speed sensor failed on the current meter at 3997 m on mooring 7. A total of 24 current meter records were available for analysis, spanning a minimum recording period of 149.2 days to a maximum of 423.3 days, with a median record length of 259.7 days. In this study we used the quality-controlled data provided by the Oregon State University (OSU) Buoy Group. Sixty-minute time-average bins of speed (cm s^{-1}), direction (°, true), u (cm s^{-1}), v (cm s^{-1}), temperature (°C) and pressure (dbar) were available.

[8] The stall percentage of the time series, current speed below rotor stall speed threshold (1.1–1.5 cm s^{-1}), varies greatly across the mooring array. In the central region (moorings 5, 6 and 7) current meter stalling represents 46% of the record length, while current meters at the western and eastern boundaries stalling represents 20% of the record length. Typically, instrument stalling was found to span 4 to 15 consecutive 60-min periods, with longer periods being a small percentage (20% for central basin moorings and 5% for western and eastern boundary moorings) of the record length. The percentage stalling of the central basin moorings excludes the 4801-m current meter on mooring 5. This current meter experienced 85% stalling over the record length, of which 63% were for periods greater than 15 hours.

[9] In the OSU Buoy Group data current meter stalls were reset to the instrument threshold value. In this study, to provide a plausible velocity range from which bottom and deep water transport estimates between the Broken and Naturaliste plateaus can be calculated the current meter stalling was dealt with in the following two ways. (1) For stall periods $\leq$15 hours we linearly interpolated the speed between good data points, and removed stall periods >15 hours from the time series. (2) Set all stall periods to 0 cm s^{-1}. Note that we have assumed that the direction from the current meter is correct when stalls occur. Similar analyses of the mooring array data were undertaken for each treatment of the stall periods in the data. This provided a velocity range for the mooring array from which the abyssal transport range into the Perth Basin was estimated. The velocity range used in this study spans estimates based on setting stall periods to the instrument threshold value or half the threshold value. The mean of the mooring array data were calculated as the weighted integral of velocity for each time series. Mooring array details and basic statistical information from the current meters are summarized in Table 1.

[10] The mean integral timescale (τ), or decorrelation timescale, of the mooring array is 10 days. The integral timescale of both the *u* and *v* velocity components adjacent to the Broken Plateau (moorings 1–3) is O(15 days), while shorter period (3–7 days) motions dominate near the Naturaliste Plateau (Table 2). The midbasin integral timescale is more variable ranging from approximately 5 to 20 days. The integral timescales of this mooring array are similar to that of the Brazil Basin and Southwest Pacific Basin mooring arrays [*Hogg et al.*, 1999; *Whitworth et al.*, 1999]. The uncertainty of the mean flow vectors were calculated as $\epsilon = \sigma(N^*)^{-1/2}$, where σ is the variance of the velocity, and N^*, the degrees of freedom of the data, was defined as $N^* = \frac{N}{2\tau}$, where N is the length of the time series [*Hogg et al.*, 1999; *Whitworth et al.*, 1999].

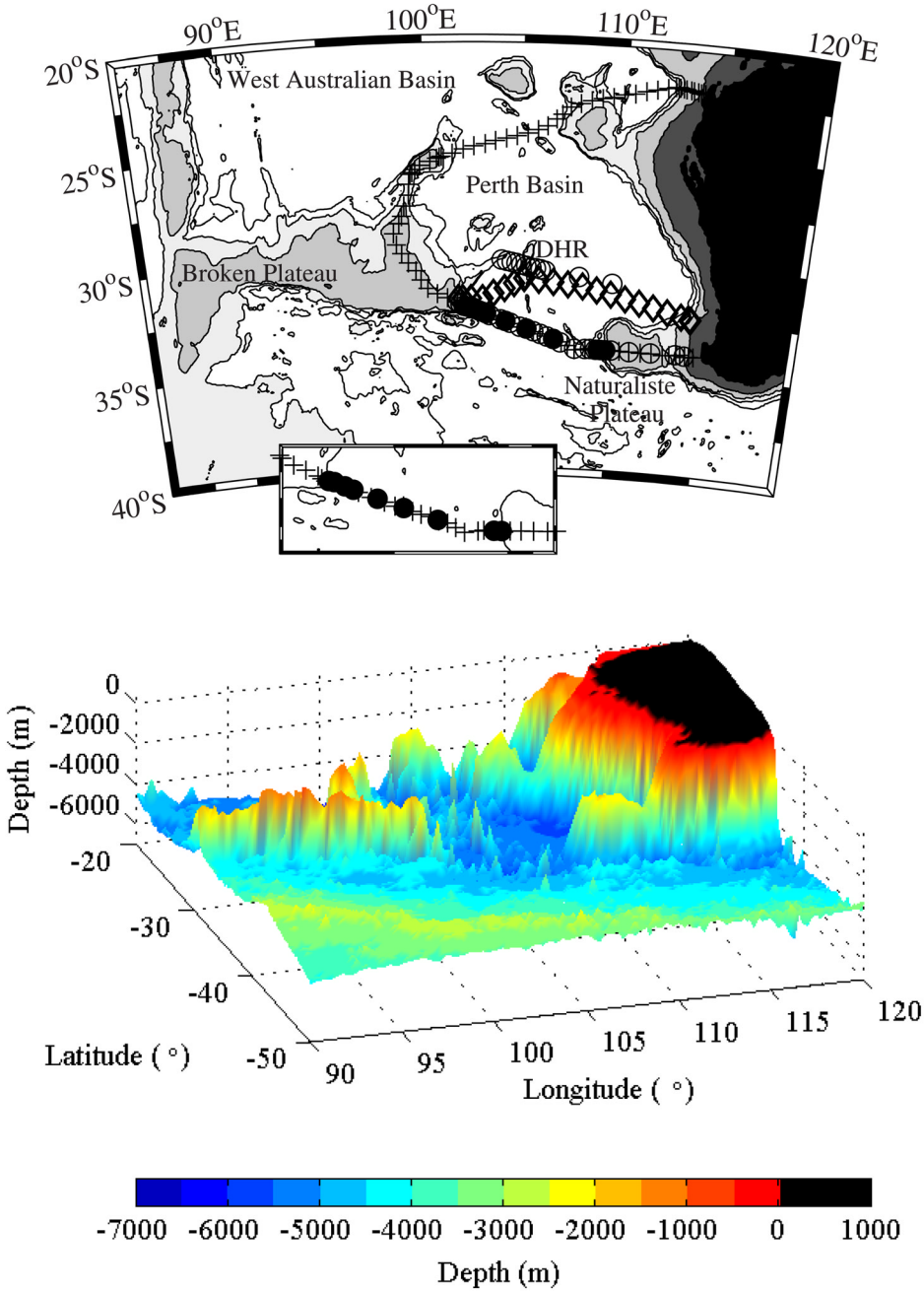

Figure 1. (top) The bathymetry of the eastern Indian Ocean defines two abyssal basins: Perth and West Australian basins. Hydrographic sections concurrent with array deployment are May 1996 (pluses) and June 1995 (circles). Also marked are the Dirk Hartog Ridge (DHR) and stations within the Perth Basin occupied by the 1995 WOCE I05E section (diamonds). The inset shows the position of recovered current meter moorings (solid circle) across the southern opening of the Perth Basin. Topography shallower than 4000 m is shaded, and the 4500-m isobath is contoured. Contour interval is 1000, 3000, 4000, and 4500. (bottom) Three-dimensional view of the Perth Basin topography from *Smith and Sandwell* [1997]. The Broken and Naturaliste plateaus constrict the southern opening of the Perth Basin. Topographic features are also found within the basin's interior.

[11] In association with the mooring array two hydrographic sections (conductivity-temperature-depth (CTD) and water analysis) were occupied in June 1995 and May 1996 (Figure 1). The June 1995 and May 1996 hydrographic sections occupied similar station positions between the Broken and Naturaliste plateaus as the earlier trans-Indian 1987 section [*Toole and Warren*, 1993]. In addition the May 1996 section surveyed the entire rim of the Perth Basin, while the June 1995 section occupied extra stations near the Dirk Hartog Ridge (105°E) (Figure 1).

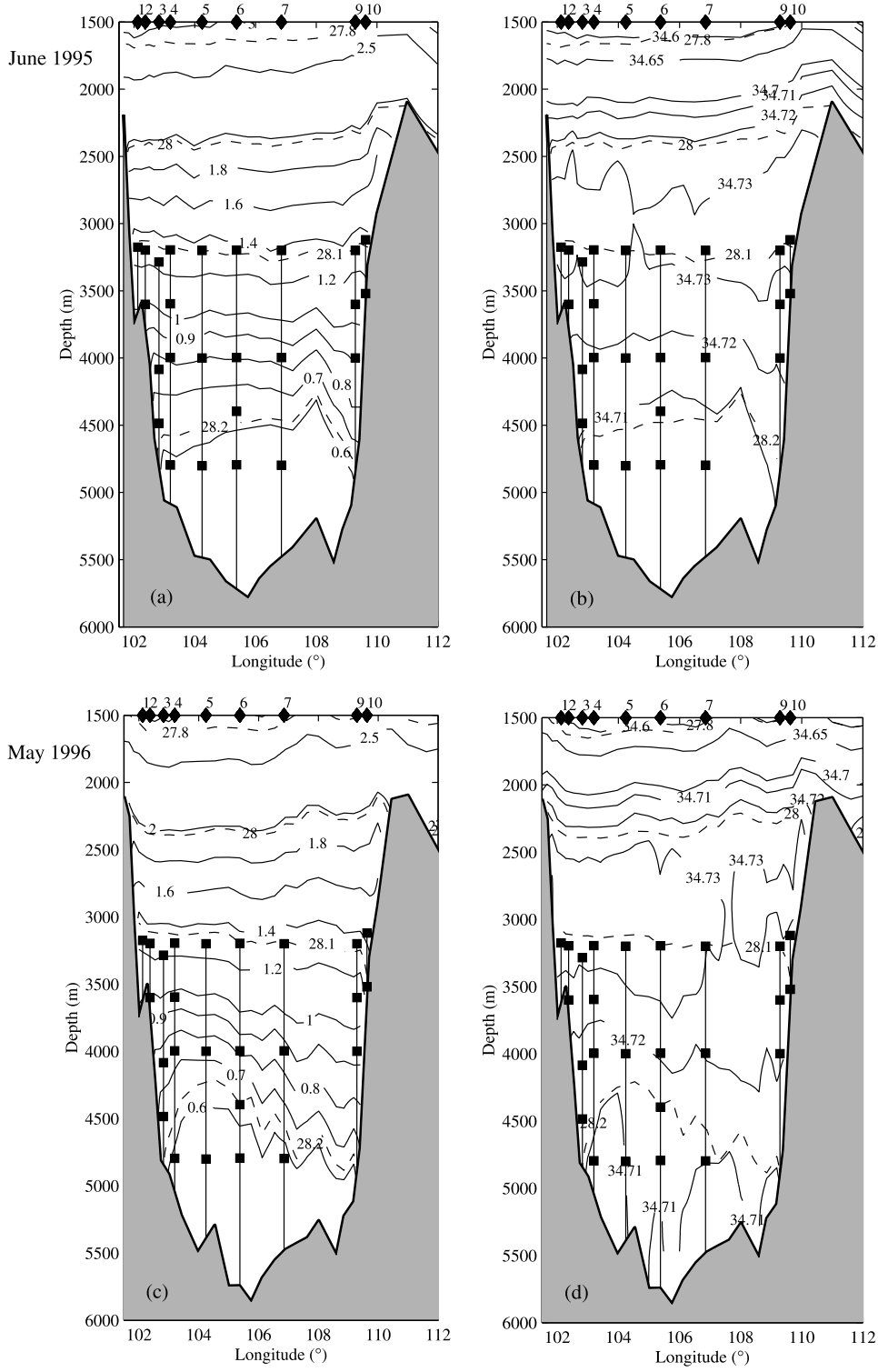

Figure 2. Property distribution between the Broken and Naturaliste plateaus for (top) June 1995 and (bottom) May 1996 hydrographic surveys (a, c) potential temperature (°C), and (b, d) salinity. Neutral density (dashed line) and vertical distribution of current meters (squares) from the recovered moorings are also shown. Mooring (recovered) numbering (1 to 10) is given along the top axis.

[12] Fifty-six stations between the Naturaliste and Broken plateaus from the *Toole and Warren* [1993] section, and the June 1995 and May 1996 surveys were used to define the Perth Basin potential temperature (θ)-salinity relationship. A second-order polynomial was used to uniquely determine the salinity from the deep Perth Basin θ-salinity data (Figure 3). An iterative process, using the polynomial fit to adjust initial salinity estimates obtained from mapping

Table 1. General Information of Location, Record Length, and Mean and Variance of Velocity and Temperature for Each Current Meter[a]

	Position					Mean			Variance		
Mooring	Latitude, °N	Longitude, °E	Start Date, dd/mm/yyyy	Record Length, days	Depth m	$\bar{u}$, cm s^{-1}	$\bar{v}$, cm s^{-1}	$\bar{\theta}$, °C	$\overline{u'^2}$, cm^2 s^{-2}	$\overline{v'^2}$, cm^2 s^{-2}	$\overline{\theta'^2}$, °C^2
1	−32.36	102.12	03/07/1995	260.4	3175	−2.69	2.83	1.148	9.11	5.65	0.002
2	−32.40	102.37	03/07/1995	227.0	3197	−4.38	2.63	1.131	10.96	12.82	0.002
2	−32.40	102.37	03/07/1995	367.8	3600	−5.35	1.95	0.871	7.71	2.83	0.002
3	−32.55	102.82	02/07/1995	243.7	3285	−0.24	1.40	1.136	14.06	14.16	0.003
3	−32.55	102.82	02/07/1995	292.2	4085	−1.05	2.05	0.666	9.70	15.02	
3	−32.55	102.82	02/07/1995	243.4	4485	−1.63	1.92	0.593	9.46	14.12	
4	−32.67	103.20	02/07/1995	259.7	3196	−0.20	1.32	1.129	4.50	13.05	0.001
4	−32.67	103.20	02/07/1995	279.4	3596	−0.35	2.11	0.871	6.77	12.41	0.002
4	−32.67	103.20	02/07/1995	233.8	3996	−1.65	3.26	0.676	6.73	12.67	0.002
4	−32.67	103.20	02/07/1995	233.0	4796	−2.27	3.07	0.562	9.12	12.21	
5	−33.00	104.24	01/07/1995	423.3	3200	2.41	−0.53	1.156	6.16	3.86	
5	−33.00	104.24	01/07/1995	349.3	4000	1.05	−0.61	0.789	0.60	1.01	
5	−33.00	104.24	01/07/1995	215.3	4801	1.00	0.50	0.565	1.30	1.45	
6	−33.34	105.38	26/06/1995	274.1	3197	1.11	0.53	1.260	2.60	1.55	
6	−33.34	105.38	26/06/1995	266.0	3997	0.42	0.26	0.718	3.60	2.54	
6	−33.34	105.38	26/06/1995	238.5	4397	0.02	−0.02	0.578	6.89	2.45	
6	−33.34	105.38	26/06/1995	258.4	4797	−0.70	−0.98	0.536	10.75	3.93	
7	−33.77	106.85	24/06/1995	338.2	3200	0.55	−0.22	1.364	1.53	2.09	0.003
7	−33.77	106.85	24/06/1995	427.1	3997	NC	NC	0.823	NC	NC	0.002
7	−33.77	106.85	24/06/1995	149.2	4797	3.71	−0.35	0.536	20.89	10.07	
9	−34.17	109.29	21/06/1995	395.5	3200	1.74	−1.68	1.166	3.99	9.88	
9	−34.17	109.29	21/06/1995	225.5	3600	0.85	−3.34	0.983	4.03	9.05	0.001
9	−34.17	109.29	21/06/1995	170.3	4000	1.65	−2.29	0.839	2.67	10.16	
10	−34.17	109.63	21/06/1995	253.5	3120	0.39	−3.44	1.286	5.38	48.41	0.007
10	−34.17	109.63	21/06/1995	252.3	3520	−1.24	−3.44	1.008	4.15	28.05	0.003

[a]On mooring 7 the speed sensor of the current meter at 3997 m failed. Mean and variance of velocity were not calculated (indicated by NC) for this instrument. Only potential temperature variance greater than 0.001°C^2 is given.

CTD salinity to current meter position and depth, determined the salinity data associated with the current meter temperature time series. The potential temperature time series associated with the velocity record was then calculated from the mooring array temperature, salinity and pressure data (Figure 3).

3. Velocity and Transport

[13] The current meter data have been low-pass filtered to remove frequencies higher than 33 hours. This frequency cutoff was based on spectral analysis of the current meter time series which showed a distinct spectral gap at this period. The current meter time series data between the Broken and Naturaliste plateaus shows predominantly northward currents near the basin's western boundary (Figure 4a), apart from initial southward flow between July and September 1995, and southward currents at the eastern boundary (Figure 4b). Weaker directionally variable currents are found in the center of the basin (Figures 4c and 4d). Vertical coherency of current speed and direction is greatest at the moorings adjacent to the Broken and Naturaliste plateaus (Figures 4a and 4b), while the central moorings (6 and 7) show the least depth dependency and have periods of enhanced bottom velocities. In the following sections we present the adjusted geostrophic and quasi-synoptic current meter transport estimates coincident with the June 1995 hydrographic survey, and the record-mean velocity of the mooring array and resultant deep transport estimates for the Perth Basin.

3.1. Adjusted Geostrophic and Quasi-Synoptic Current Meter

[14] Two hydrographic sections (June 1995 and May 1996) between the Broken and Naturaliste plateaus were concurrent with the mooring array. Unfortunately, a number of current meters had failed by May 1996; therefore adjusted geostrophic transport estimates were computed for only the June 1995 survey. The property distribution (Figure 2) defines the boundary between northward flowing AABW and LCDW, and overlying southward flowing Indian Deep Water (IDW). AABW and LCDW are characterized by $\theta \leq$

Table 2. Integral Timescale of Mooring Array Grouped by Depth[a]

	Mooring																	
	1		2		3		4		5		6		7		9		10	
Depth, m	*u*	*v*	*u*	*v*	*u*	*v*	*u*	*v*	*u*	*v*	*u*	*v*	*u*	*v*	*u*	*v*	*u*	*v*
3200	20.6	12.3	6.9	14.0	16.3	15.2	9.5	9.7	34.0	22.9	9.9	12.9	8.6	13.6	6.8	7.9	2.4	9.6
3500			15.1	15.5			7.5	7.3							2.7	6.9	1.3	3.9
4000					10.4	10.9	4.6	5.3	14.5	14.4	9.4	7.4	NC	NC	5.6	9.1		
4400					8.5	5.4					8.3	5.9						
4800							3.5	3.8	5.4	19.9	9.5	3.8	10.4	7.2				

[a]Time unit is days. NC, not calculated.

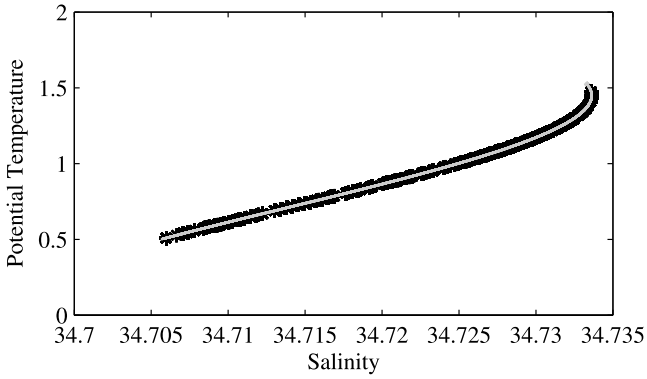

Figure 3. Perth Basin deep potential temperature (θ)-salinity relationship (solid line) defined from hydrographic stations between the Broken and Naturaliste plateaus and mooring array θ data and uniquely defined salinity data (star).

2°C, a slight salinity maximum and higher oxygen concentration (not shown) than overlying IDW. The boundary between these water masses is defined by neutral density (γ^n) = 28.0 kg m^{-3}. CTD data were used to calculated the geostrophic velocity relative to γ^n = 28.0 kg m^{-3}. Relative velocity distribution between the Broken and Naturaliste plateaus show northward and southward flow adjacent to the western and eastern boundaries, respectively, and alternating bands of northward and southward relative velocity in the central basin (Figure 5a).

[15] Adjusted relative velocities (Figure 5b) across the deep basin were determined by minimizing the difference between the relative geostrophic velocity from station pairs that straddled a mooring and the 5-day low-pass filtered time series data at the time of the hydrographic survey. The velocity adjustments were then linearly interpolated across the basin (Figure 5c, squares). Velocity adjustments for relative velocity straddling moorings 5, 6, 7 and 9 are −0.01 cm s^{-1}, −0.42 cm s^{-1}, −5.48 cm s^{-1} and 2.11 cm s^{-1}, respectively (Figure 5c, squares). Linear interpolation to CTD station pairs between moorings 6, 7

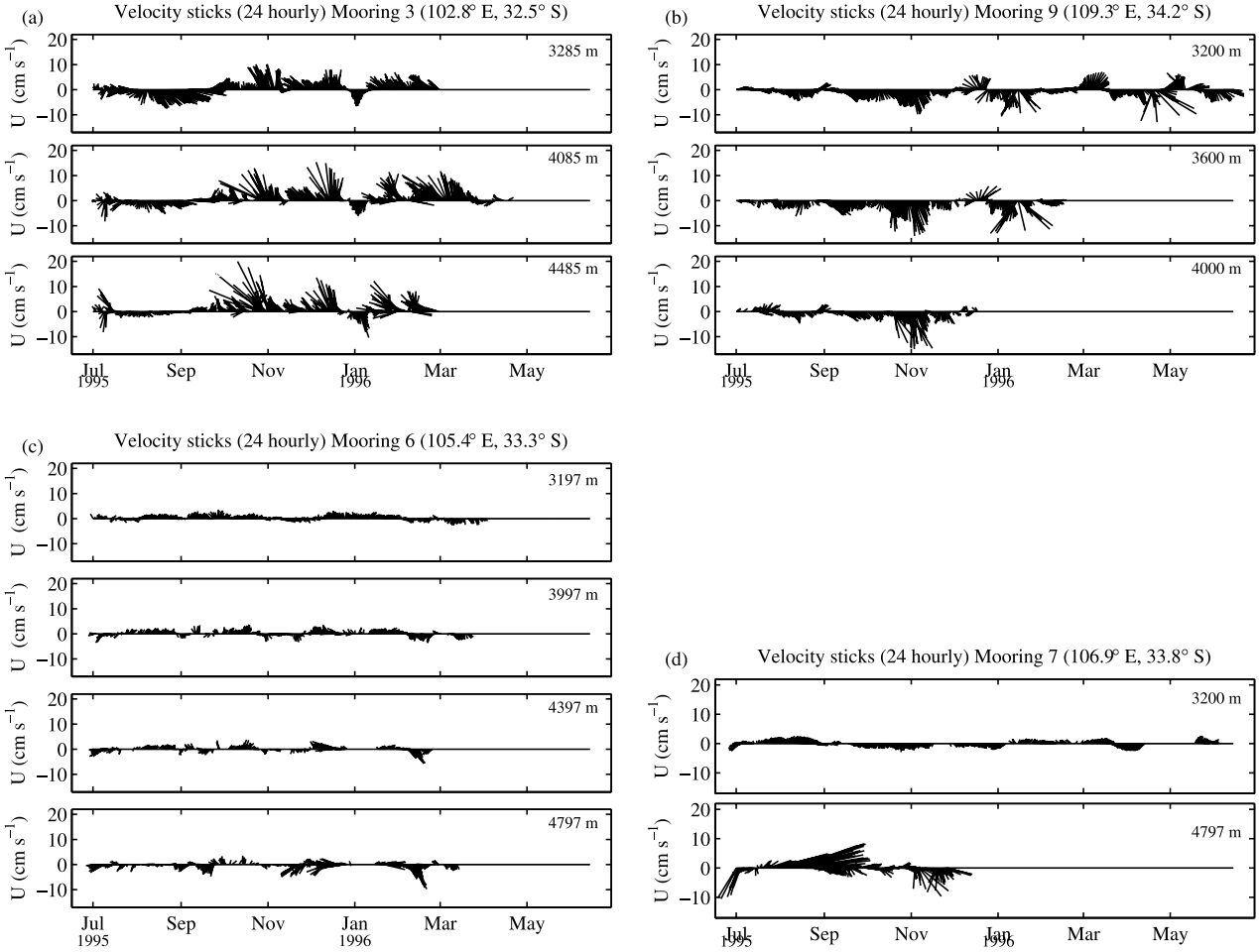

Figure 4. Vector horizontal velocities (cm s^{-1}) as a function of time at moorings spanning the southern opening of the Perth Basin. (a) Mooring 3 on the western boundary, (b) mooring 9 on the eastern boundary, and in the middle of the basin, (c) mooring 6 and (d) mooring 7. Northward velocity is positive, and depth (m) of each instrument is given. Instrument stall periods of 15 hours or less have been interpolated between surrounding data points, and periods greater than 15 hours are set to 0 cm s^{-1}. Data have been low-pass filtered to remove frequencies higher than 33 hours.

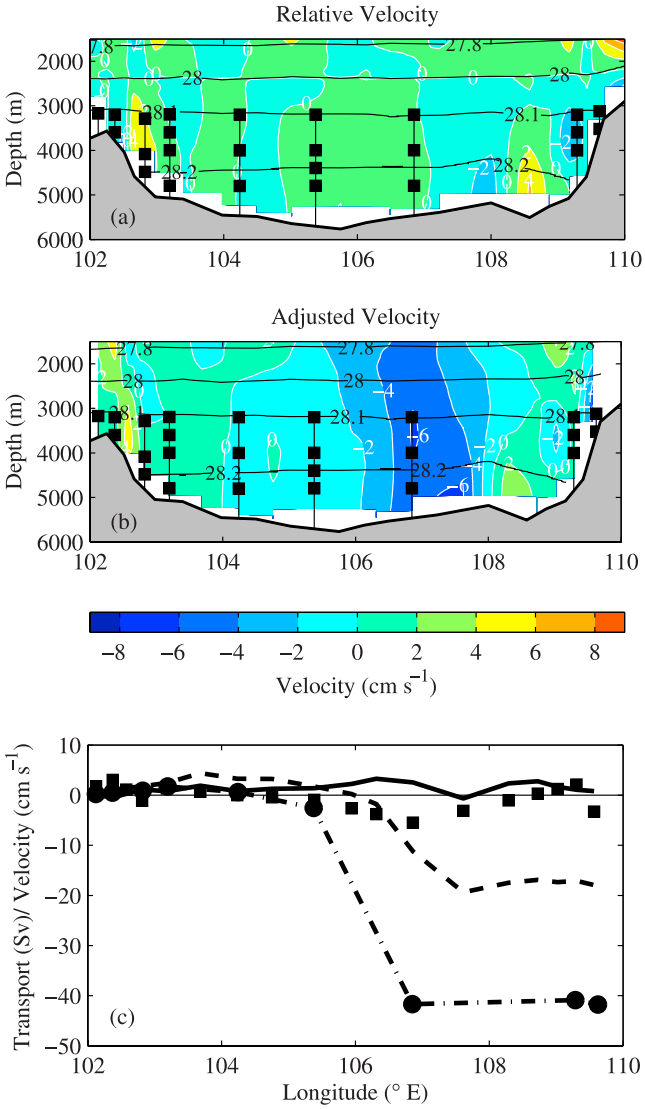

Figure 5. (a) Geostrophic velocity relative to γ^n = 28.0 kg m^{-3} from the June 1995 hydrographic section and (b) adjusted velocity based on current meter data. Positive velocity is northward. (c) Cumulative transport (Sv) from the Broken Plateau to the Naturaliste Plateau below γ^n = 28.1 kg m^{-3} for June 1995 from hydrographic and current meter data. Geostrophic transport relative to γ^n = 28.0 kg m^{-3} (solid line), adjusted geostrophic transport (dashed line), and 5-day low-pass filtered direct transport (dash-dotted line, circle). Also shown are the basin interpolated station pair velocity adjustments (squares, cm s^{-1}) that were applied to the relative geostrophic velocity.

and 9 result in southward velocity adjustments across the interior of the Perth Basin. The velocity adjustment is dominated by the large southward velocity at 4797 m on mooring 7 at the time of the June 1995 section (Figure 4d). In the time series data this mooring shows periods of bottom trapped strong southward and northward velocity. The velocity sensor on the current meter at 3997 m failed thereby limiting our ability to determine the decay height above bottom of these velocity features. Bottom intensified velocities in the time series indicate the existence of variability whose spatial and vertical scales, period and forcing are not resolved by this mooring array. These data suggest that the central basin abyssal flow is not quiescent.

[16] The adjusted relative velocity has northward velocity between the Broken Plateau and 104°E, with strongest velocity adjacent to the plateau, and weak southward velocity confined to the slope of the Naturaliste Plateau (Figure 5b). The most dramatic change between the relative and adjusted velocity distributions is found in the center of the basin. Weak relative southward flow is found between 104°E and 106°E, while between 107°E and 109°E the relative velocity is dominated by alternating strong southward and slightly weaker northward velocities. Linear interpolation of the velocity adjustments across the basin strengthens the southward velocity between 107°E and 108°E. Unfortunately, mooring 8 (109°E, 34.77°S) that was deployed in the region of northward relative velocity was not recovered. Therefore the adjusted velocity applied to this region was derived from an interpolation between the strong southward velocity at mooring 7 and weak northward velocity at mooring 9.

[17] The adjusted relative velocity distribution and 5-day low-pass filtered direct velocity at June 1995 are used to estimate the quasi-synoptic basin transport below γ^n = 28.1 kg m^{-3}. A constant relative velocity shear was assumed to extend the relative velocity to the sea floor. The adjusted relative transport is a combination of the baroclinic and barotropic transports. The barotropic transport is the basin interpolated velocity adjustments applied to the station pair area below γ^n = 28.1 kg m^{-3}. The direct transport is the current meter velocity applied to the distance between mooring pairs and depth between current meter instruments on each mooring, except for moorings 7 and 9. Mooring 9's velocity time series is representative of the western edge of the narrow boundary current (*Toole and Warren* [1993], and Figures 2 and 5) and not of the velocity in the central basin. Therefore the direct velocity estimates from mooring 7 were applied to within a Rossby radius of mooring 9.

[18] The adjusted relative and direct transport estimates between the Broken Plateau and 105.5°E, and at the eastern edge of the basin (east of 107°E) are similar (Figure 5c). The difference in the cumulative basin transport between the adjusted relative (−17.9 Sv) and direct (−41.8 Sv) transport estimates results from applying the large southward velocity at 4797 m on mooring 7 to the significant area of the Perth Basin east of 106°E (Figure 5). We speculate that much of the midbasin southward transport in both the adjusted and direct transport estimates should have been balanced by northward flow further east (near 108.5°E). Once again we lament the non-recovery of mooring 8. We conclude that the quasi-synoptic and adjusted cumulative transport estimates for June 1995 contain significant errors and are therefore unreliable.

[19] The transport estimates from the adjusted geostrophic and current meter quasi-synoptic velocity are found to be severely compromised by the nonrecovery of mooring 8 and application of the velocity of mooring 7 to a large area of the central Perth Basin. At longer timescales (≥2 months) the velocity of mooring 7 is not dominated by the short timescale velocity fluctuation coincident with the June 1995 hydrographic survey. Given this, the record-mean velocity

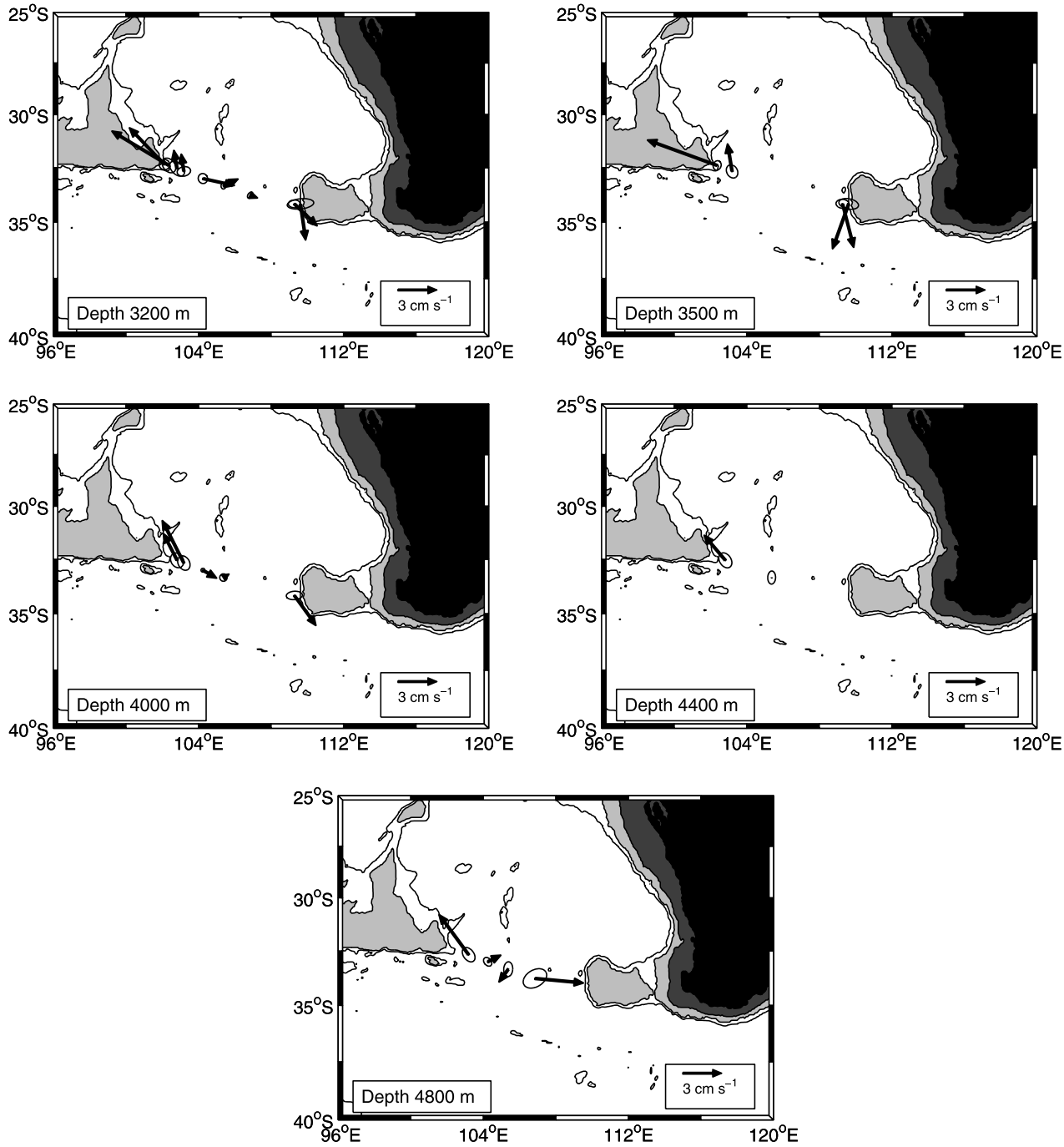

Figure 6. Mean flow vectors (cm s^{-1}) with standard error ellipse as a function of depth between the Broken and Naturaliste plateaus. The error ellipse is calculated from the velocity variance ellipse reduced in size by the square root of the number of degrees of freedom (section 2). Moorings numbering is given in Figure 2. The 4000-m isobath is contoured, and topography shallower than 3000 m is shaded.

at 4797 m on mooring 7 provides an accurate estimate of the long-term velocity at the mooring location. In the following sections we assume that the record-mean velocity at mooring 7 provides a reliable estimate of the time-mean velocity for the central Perth Basin from which transport can be estimated.

3.2. Record-Mean Current Meter

[20] Record length mean flow vectors show northward velocity at the western edge of the Perth Basin, and southward velocity at the eastern boundary (Figure 6). In the central region (104°E–108°E) the flow is weaker and vertically less consistent than that at the basin boundaries, while between 4000 m and 4800 m velocity vectors increase toward the bottom indicating bottom flow enhancement.

[21] Total transport estimates across the basin for $\gamma^n \geq 28.1$ kg m^{-3} range between 4.4 to 5.8 Sv (Figure 7). The transport range results from the application of the two methods chosen to deal with current meter stalling in the time series. Grouping the current meters by depth and

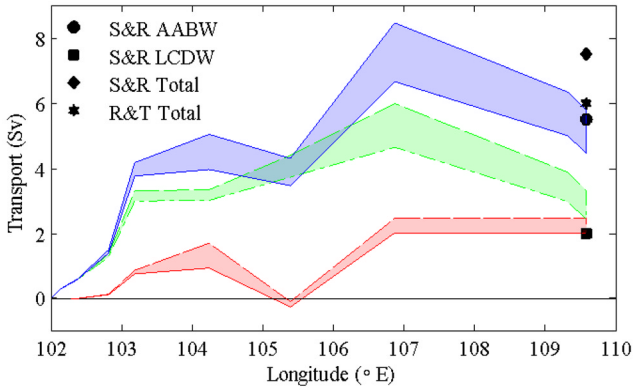

Figure 7. Cumulative net mean transport range (blue, Sv) from the mooring array between the Broken and Naturaliste plateaus. Net transport is divided into two Southern Ocean water masses that enter the basin: LCDW (green) and AABW (red). Also shown are Perth Basin total and water mass transport estimates from *Robbins and Toole* [1997] (star), and *Sloyan and Rintoul* [2001] (diamond, square and circle).

density class provides direct transport estimates for two Southern Ocean origin water masses: Lower Circumpolar Deep Water ($28.1 \leq \gamma^n \leq 28.2$ kg m^{-3}) and Antarctic Bottom Water ($\gamma^n \geq 28.2$ kgm^{-3}) (Figure 2). Basin LCDW and AABW transport ranges are 2.4 to 3.3 Sv and 2.0 to 2.5 Sv, respectively. Much of the net northward transport of LCDW is achieved within 1° of longitude of the Broken Ridge (Figure 7). Northward transport of LCDW in the central basin is balanced by southward transport at the eastern boundary. Northward transport of AABW extends from the western boundary to 104.5°E. In the middle of the basin compensating southward and northward transport is found. The AABW southward transport results from a mean southward velocity at mooring 6 (Figure 4c), while east of 106°E compensating northward transport results from a mean northward velocity at mooring 7 (Figure 4d).

[22] The transport estimates from the current meter data agree within errors with previous inverse based estimates of bottom and deep water transport between the Broken and Naturaliste plateaus (Figure 7) [*Robbins and Toole*, 1997; *Sloyan and Rintoul*, 2001]. Across the Perth Basin, *Robbins and Toole* [1997] grouped LCDW and AABW (as defined by this study) into one layer ($\gamma^n \geq 28.1$ kg m^{-3}) and imposed a 6 Sv northward transport constraint on the layer (based on transport estimate below 2000 m from *Toole and Warren* [1993]). When compared to the direct transport estimates of this study, *Sloyan and Rintoul* [2001] overestimate the northward transport of AABW and underestimate the northward transport of LCDW across the southern boundary of the Perth Basin. Their total northward transport below $\gamma^n \geq 28.1$ kg m^{-3} was 7.5 Sv.

4. Diapycnal Velocity and Diffusivity

4.1. Property Conservation

[23] In the Perth Basin water of $\gamma^n \geq 28.2$ kg m^{-3} is confined to the southern and southeastern region of the basin (Figure 8). The surface area and extent of $\gamma^n =$ 28.2 kg m^{-3} and $\theta = 0.64$°C north of 32°S are similar ($\leq$2% difference) within the basin (Figure 8). Therefore estimates of diapycnal velocity and diffusivity across $\gamma^n =$ 28.2 kg m^{-3} can be approximated using the $\theta = 0.64$°C isotherm surface.

[24] We estimate the deep mixing rate across $\theta = 0.64$°C ($\gamma^n = 28.2$ kg m^{-3}) for the Perth Basin from the layer temperature budget [e.g., *Hogg et al.*, 1982; *Whitehead and Worthington*, 1982; *Morris et al.*, 2001]. Assuming a steady-state heat balance,

$$\int_v \nabla \cdot (U\theta)\, dV = \int_v (\kappa\theta_z)_z dV, \tag{1}$$

where V is a volume bounded at the top and bottom by isothermal (density) surfaces or the seafloor, U is the three-dimensional flow field, and κ is the vertical diffusivity [*Morris et al.*, 2001]. Equation (1) can be rewritten as

$$\int_A U\theta \cdot n\, dA = \left[\overline{\kappa\theta_z} A\right]_{m+1} - \left[\overline{\kappa\theta_z} A\right]_m, \tag{2}$$

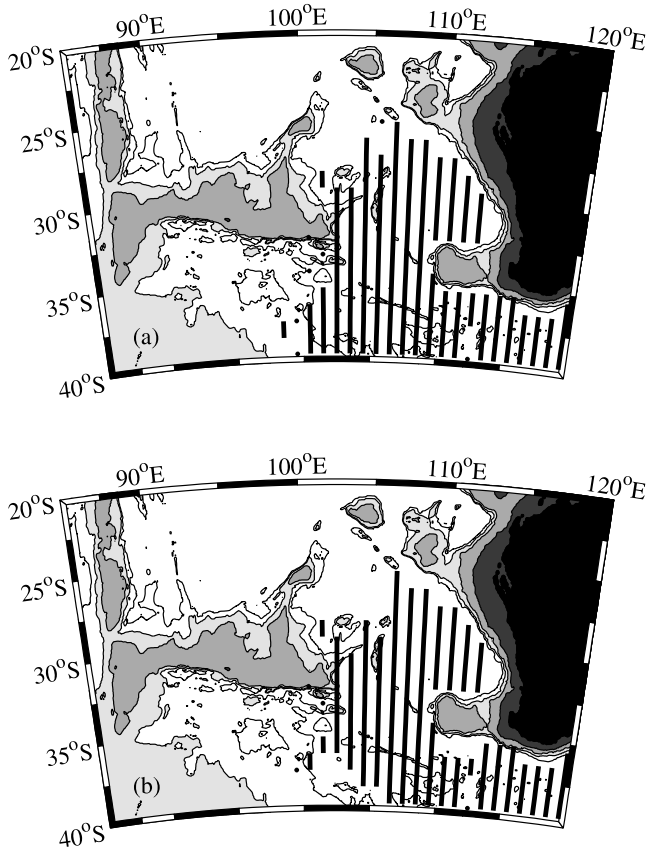

Figure 8. (a) Northward extent of the $\gamma^n = 28.2$ kg m^{-3} surface (hatched) and (b) $\theta = 0.64$°C surface (hatched) in the Perth Basin. The source of AABW is confined to the South Australian Basin north of 40°S. Neutral density and potential temperature for the eastern Indian Ocean were calculated from the Hydrobase Climatology (www.whoi.edu/science/PO/hydrobase). Topography shallower than 4000 m is shaded, and the 4500-m isobath is contoured. Contour interval is 1000, 3000, 4000, and 4500.

Table 3. Property and Mixing Estimates for AABW[a]

AABW	θ, °C	Surface Area, $\times 10^{11}$ m^2	$\overline{\theta_z}$, $\times 10^{-4}$ °C m^{-1}	Advection Mass, Sv	Diffusive Temperature, °C Sv	w*, $\times 10^{-6}$ m s^{-1}	κ_θ, $\times 10^{-4}$ m^2 s^{-1}	Diffusive Heat Flux, W m^{-2}
Perth Basin	0.64	8.0	2.4	2.0–2.5	0.24–0.27	2.5–3.1	13–15	1.2–1.4
Somali Basin	1.12	30.0	3.9	4.0 ± 1.0	NC	1.3	10.6 ± 2.7	NC
Brazil Basin	0	4.5	13.0	2.4	0.3	5.2 ± 2.1	5.1 ± 30.0	2.7 ± 1.1
	0.8	56	17.0	3.7	3.13	0.7 ± 0.3	3.3 ± 1.6	2.3 ± 1.1
Scotia Sea	−0.25	7.0	2.7	4.0	NC	5.7	39	NC

[a]Perth Basin data are relative to the θ = 0.64°C surface. Within the Perth Basin this isotherm is coincident with the γ^n = 28.2 kg m^{-3} surface. Property area and temperature gradient are calculated from the Indian Ocean Hydrobase climatology. Somali Basin data are for θ = 1.12°C (4000 m) from *Barton and Hill* [1989]. Brazil Basin data are for θ = 0.0°C and θ = 0.8°C from *Morris et al.* [2001]. Scotia Sea data are for θ = −0.25°C from *Heywood et al.* [2002]. NC, not calculated.

where A is the surface area of volume V, n is the normal vector, $\kappa\overline{\theta_z}$ is the area averaged potential temperature gradient and diffusivity of the bounding isotherms (or density), and m, $m + 1$ are the bounding isothermal (or isopycnal) surfaces of the layer. The left-hand side of equations (1) and (2) represents the lateral fluxes into and out of the layer, and cross-isothermal (diapycnal) fluxes through the upper and lower boundaries of the layer. Lateral volume and potential temperature fluxes were estimated from the velocity range of the current meter and potential temperature time series. Cross-isothermal (diapycnal) velocity is derived from mass conservation. The area of the θ = 0.64°C surface and vertical potential temperature gradient surrounding the isothermal surface were calculated using the Hydrobase climatology (www.whoi.edu/science/PO/hydrobase). Diapycnal velocity (w*), diffusivity (κ) and diffusive heat flux across AABW (θ = 0.64°C/γ^n = 28.2 kg m^{-3}) layer are found to range between 2.5–3.1 × 10^{-6}m s^{-1}, 13–15 × 10^{-4} m^2 s^{-1}, and 1.2–1.4 W m^{-2}, respectively (Table 3). (The range of the mixing estimates is derived from the mean transport range of the mooring array.) Consideration of the geothermal heat flux of 50 × 10^{-3} W m^{-2} [*Stein et al.*, 1995] does not substantially change the estimated range of κ, and has not been considered in this study.

[25] In the Brazil Basin area averaged AABW (θ = 0 and 0.8°C) upwelling rates, diffusivity and diffusive heat flux are comparable with the Indian Ocean's Perth and Somali basins and Scotia Sea estimates (Table 3). AABW upwelling rate in the Perth Basin (θ = 0.64°C) is half that of upwelling across θ = 0°C in the Brazil Basin and in the Scotia Sea. Note that both the Perth and Brazil basins have similar mass advection but the isothermal area is halved between the two basins, while advection into the Scotia Sea is twice that of the Perth Basin. In the Somali Basin (western equatorial Indian Ocean) the θ = 1.12°C surface occupies a much larger area than θ = 0.64°C in the Perth Basin resulting in an upwelling rate that is half that of the Perth Basin. Perth Basin area-averaged abyssal diffusivity estimates are approximately 2 to 3 times larger than estimates in the Brazil Basin [*Hogg et al.*, 1982; *Polzin et al.*, 1997; *Morris et al.*, 2001], 3 times smaller than mixing estimates of the Scotia Sea [*Heywood et al.*, 2002], and similar to diffusivity estimates in the Somali Basin. Area averaged abyssal diffusivity rates in the Perth Basin (Somali Basin and Scotia Sea) are more typical of diffusivity values over rough topography and within deep sills in the ocean ridges [*McCarthy et al.*, 1997; *Polzin et al.*, 1997; *Ferron et al.*, 1998; *Naveira Garabato et al.*, 2004].

[26] Previous estimates of Indian Ocean diapycnal velocity and diffusivity are given in Table 4. These estimates, apart from those of *McCarthy et al.* [1997], are derived from basin-scale property budgets for varying latitudinal limits of the Indian Ocean (e.g., north of 32°S, between 32°S and 18°S and north of 8°S), neutral density surfaces, and depth surfaces. The *McCarthy et al.* [1997] mixing estimates are based on geostrophic transport calculations relative to 1650 m within the confines of a deep sill in the Ninetyeast Ridge at 28°S. A deeper reference level results in a transport reduction of bottom water through the sill and suggests that the diffusivity may be too large [*Warren and Johnson*, 2002].

[27] Perth Basin AABW diapycnal velocity and diffusivity estimates (Table 3, Perth Basin) are larger than Indian Ocean diapycnal velocity and diffusivity estimates, but smaller than mixing values near deep sills of the Ninetyeast Ridge (Table 4). The Indian Ocean mixing estimates (Table 4) are consistent with each other, and 4 to 10 times larger than basin average mixing estimates for the Pacific Ocean north of 32°S [*Whitworth et al.*, 1999]. All of the mixing estimates are based on basin property conservation principles, but this method has been applied to disparate spatial scales. The cascade of lower to higher mixing rates with large to smaller spatial scale is due to the isolation of Indian Ocean mixing "hot spots" to individual basins and sills in which much of the mixing occurs. The

Table 4. Previous Diapycnal Mixing Estimates for the Indian Ocean[a]

Study	Diapycnal Velocity, m s^{-1}	Diffusivity, m^2 s^{-1}	Comments
Warren [1981]	4 × 10^{-7}	NC	north of 18°S; across 2000 m
Toole and Warren [1993]	7 × 10^{-7}	NC	north of 32°S; across 2000 m
Robbins and Toole [1997]	4.5 × 10^{-7}	NC	north of 32°S; across 2000 m
Sloyan and Rintoul [2001]	O(10^{-6})	NC	between 32°S and 18°S; 27.8 ≤ γ^n ≤ 28.2
Ganachaud et al. [2000]	1–3 × 10^{-7}	2–10 × 10^{-4}	average (three boxes) for deep water layers north of 32°S; extreme mixing values found north of 8°S
McCarthy et al. [1997]	4–33 × 10^{-6}	13–105 × 10^{-4}	deep sill in Ninetyeast Ridge at 28°S

[a]NC, not calculated for given study.

magnitude difference of mixing estimates indicates that mixing in the ocean is not spatially uniform and suggests that mixing is enhanced in certain regions.

4.2. Strain

[28] To determine diffusivity from the CTD profile data we apply the scaling formula for estimating the dissipation of turbulent kinetic energy (ϵ) based on finescale strain (ξ) [*Wijesekera et al.*, 1993],

$$\epsilon_\xi = 7 \times 10^{-10} \frac{\langle N^2 \rangle}{N_o^2} \frac{\langle \xi_z^2 \rangle^2}{\left[\xi_{GM}^2\right]^2} \text{ W kg}^{-1}, \quad (3)$$

where N_o (buoyancy frequency) is the reference N used in [*Garrett and Munk*, 1975] (hereinafter referred to as GM), 7×10^{-10} W kg^{-1} is the dissipation in the background GM wave field at $N = N_o$ (= 5.2×10^{-3} rad s^{-1}) and 30° of latitude; ξ_{GM}^2 is the strain variance of the modified GM wave field [*Cairns and Williams*, 1976], and ξ_z^2 is the strain variance of the internal wave field. Angle brackets denote some averaging process. The relationship between the dissipation rate of turbulent kinetic energy (ε) and buoyancy flux is [*Osborn*, 1980]

$$\epsilon = \Gamma^{-1} \kappa_z N^2 \quad (4)$$

or in terms of diffusivity

$$\kappa_z = \Gamma \frac{\epsilon}{N^2}, \quad (5)$$

where $\Gamma = 0.2$ is the mixing efficiency. Substitution of ϵ_ξ into equation (5) gives an expression for κ from strain variance [*Sloyan*, 2005]. *Mauritzen et al.* [2002], *Kunze* [2003] and *Sloyan* [2005] have applied this method to CTD data for various oceanic regions.

[29] As in the work by *Sloyan* [2005], ξ_z is calculated from CTD data where it is assumed that large vertical length scales in the density profiles represent the time mean ($\overline{N^2}$) and small vertical length scales represent the internal wave field (N^2). In this study $\overline{N^2}$ is calculated over 500 m. The vertical length scale ($\Delta Z = \frac{\lambda_z}{2}$) for calculation of N^2 was determined by spectral analysis of the vertical density profiles in the Perth Basin data (Figure 1). The power spectra were flat for wave lengths longer than λ_z = 60–80 m. At smaller wave lengths the power spectra were dominated by noise. Therefore N^2 for the internal wave field was calculated over ΔZ = 40 m. Vertical profiles of $\overline{N^2}$ and N^2 over their respective vertical interval are estimated as linear fits to the specific volume anomaly depth profiles using the adiabatic leveling method [*Bray and Fofonoff*, 1981; *Mauritzen et al.*, 2002].

[30] Diffusivity estimates from hydrographic data between the Broken and Naturaliste plateaus, in the interior of the Perth Basin, and at the northern boundary of the Perth Basin are O(10^{-4} to 10^{-3} m^2 s^{-1}) below 4000 m (Figure 9). The three hydrographic sections (Figures 9a, 9b, and 9c) across the southern opening of the Perth Basin span a decade. They provide a consistent view of the vertical diffusivity. All section realizations show a marked increase in diffusivity below 4000 m. The largest diffusivity values are found between 103°E and 108°E coincident with the northward transport of AABW into the basin. In the interior of the Perth Basin (Figures 9d and 9e), diffusivity values are smaller than diffusivity at the southern opening of the basin, although diffusivities of O(10^{-4} m^2 s^{-1}) are observed within 500 m of the bottom near topographic features. Bottom intensified diffusivity values at the northern boundary of the Perth Basin (Figure 9f) are similar to those found at the southern opening of the basin.

[31] Strain-based diffusivity estimates for hydrographic sections within and at the boundary of the Perth Basin show that mixing is spatially variable in the basin. High mixing rates are found at the boundary of the Perth Basin and near topographic features in the interior of the basin. The largest mixing values are found across the southern opening of the basin. The spatially variable mixing in the Perth Basin is able to support area average AABW mixing of O(10^{-3} m^{2}s^{-1}). Perth Basin area averaged abyssal diffusivity of O(10^{-3} m^2 s^{-1}) is an order of magnitude larger than that found in the South Atlantic Brazil Basin.

5. Abyssal Mixing in the Perth Basin and Implications for the Indian Ocean Overturning Circulation

[32] The diffusive heat flux across an isothermal layer is the amount of heat required to overcome the buoyancy difference between water entering the basin and that upwelled across an upper bounding isopycnal or isotherm surface. Across a similar isotherm surface the diffusive heat flux in the Perth Basin is half that of the Brazil Basin (Table 3). In the Perth Basin the vertical temperature gradient surrounding the bounding isopycnal is an order of magnitude smaller than that in the Brazil Basin, and similar to the abyssal temperature gradient of the Somali Basin and Scotia Sea (Table 3). In the Perth Basin (Somali Basin and Scotia Sea) a smaller heat flux is needed to maintain the abyssal upwelling volume than that required in the Brazil Basin. The difference between the diffusive heat flux required to maintain the abyssal upwelling in the Indian Ocean (Scotia Sea) and South Atlantic Ocean suggests that the abyssal stratification of these oceans are sufficiently different that it is an important factor determining the overturning circulation (volume) that each basin can support for a given amount of turbulent kinetic energy.

[33] The abyssal Perth Basin stratification ($N^2 = 4–8 \times 10^{-7}$s^{-2}) is 5 times weaker than that of the Brazil Basin (Figure 10). Given equation (5), it is the difference in the abyssal stratification between the Perth and Brazil basins that results in the larger diffusivity values and smaller diffusive heat fluxes found in the Perth Basin. From equation (4) the required dissipation rate of turbulent kinetic energy for the abyssal Perth Basin is ϵ = O(10^{-9} W kg^{-1}). In the Brazil Basin $\bar{\epsilon}$ = O(10^{-9} W kg^{-1}) for AABW isopycnal surfaces [*Morris et al.*, 2001]. The turbulent kinetic energy required to maintain the Perth Basin mixing is similar to that required in the Brazil Basin even though the diffusivity is 2 to 3 times larger. As mentioned, similar values of κ in the Perth Basin are found over rough topography in the Brazil Basin, but the required dissipation rate of these areas, ϵ = O($10^{-8.5}$ W kg^{-1}) [*St. Laurent et al.*, 2001], is higher than that required in the Perth Basin. The turbulent kinetic energy required to maintain the Indian Ocean mixing is similar to that required in the Scotia Sea [*Heywood et al.*, 2002].

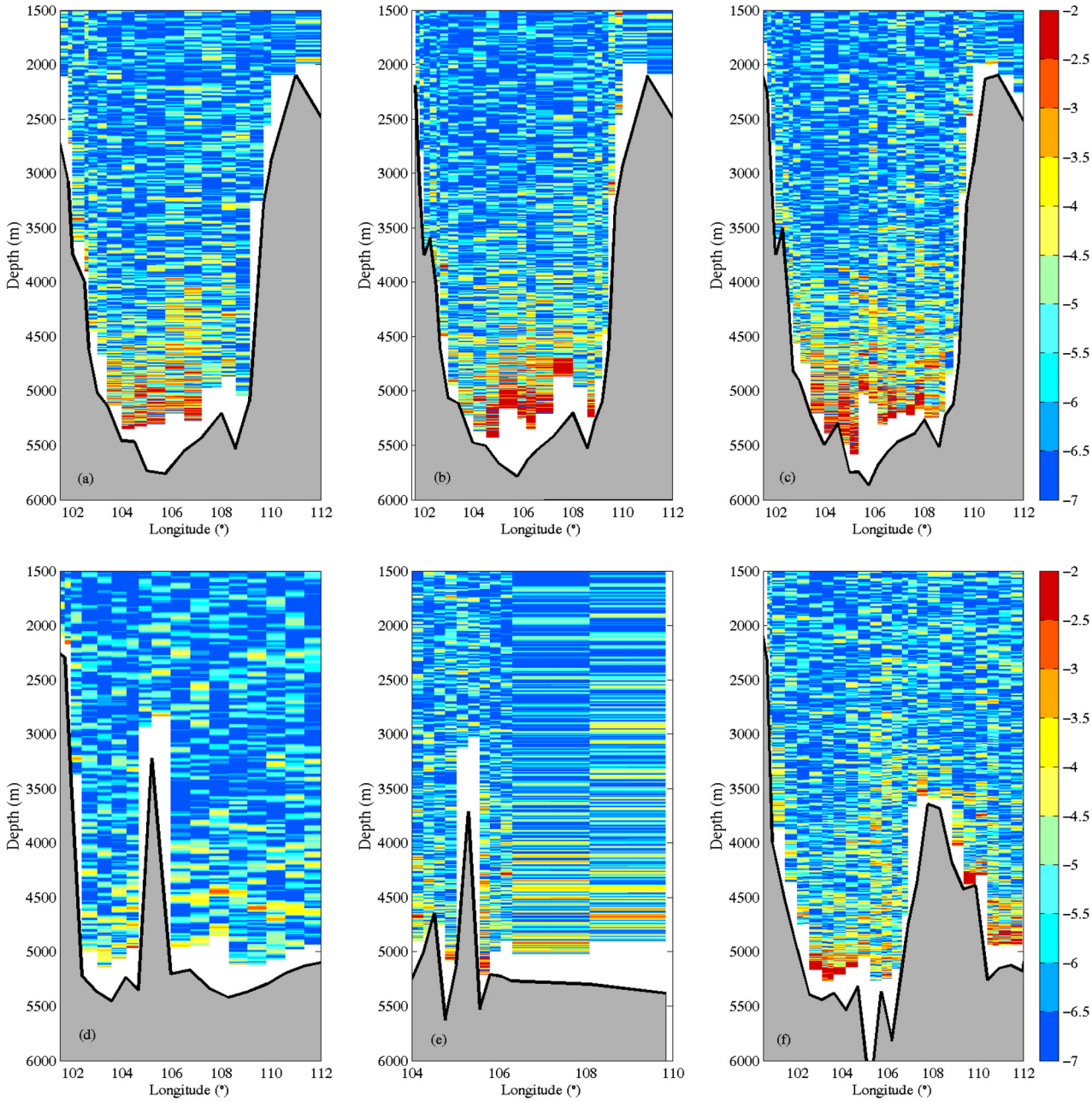

Figure 9. Vertical distribution of diffusivity ($\log_{10}$ m^2 s^{-1}) between the Broken and Naturaliste plateaus for (a) November 1987 [*Toole and Warren*, 1993], (b) June 1995, and (c) May 1996 hydrographic sections, within the Perth Basin for (d) WOCE I05E 1995 and (e) June 1995, and (f) at the northern boundary of the Perth Basin stations east of 100°E for the 1996 section. Hydrographic station positions are given in Figure 1.

[34] Direct estimates of diffusivity from basin property constraints (equation (2)) can be expressed in terms of the upwelled volume across the bounding isopycnal surface between the abyssal and deep water masses.

$$Q\Delta\theta = -\kappa\theta_z A, \tag{6}$$

where Q is the volume of water that upwells across the bounding isothermal surface, $\Delta\theta$ is the volume-flux-weighted difference in potential temperature between the incoming water and bounding isotherm, θ_z is the potential temperature gradient surrounding the bounding isotherm, and A is the area of the bounding surface within the basin. Using equation (5), the definition of the stability ratio $R_\rho = \frac{\alpha\theta_\rho}{\beta S_z}$ and $N^2 = g(\alpha\theta_z - \beta S_z)$ we have

$$Q = -\frac{\Gamma\epsilon}{g\alpha\Delta\theta}\frac{R_\rho}{(R_\rho - 1)}A, \tag{7}$$

where α is the thermal expansion coefficient, β is the haline contraction coefficient, and S_z the vertical gradient of salinity.

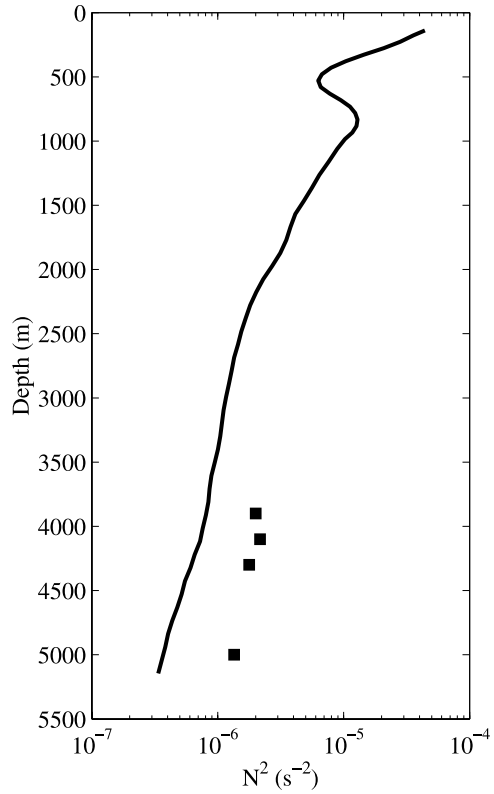

Figure 10. Vertical profile of $\overline{N^2}$ (thick line) for the Perth Basin. $\overline{N^2}$ was calculated from Indian Ocean Hydrobase climatology. Also shown (black squares) are $\overline{N^2}$ for the Brazil Basin from *Morris et al.* [2001].

[35] Equation (7) states that the overturning rate (Q) is related to the dissipation of turbulent kinetic energy and potential temperature difference between the incoming abyssal water and the overlying isotherm boundary. For a given amount of turbulent kinetic energy, abyssal basins in which a small potential temperature difference exists between the incoming and upwelling water can support a larger overturning circulation than basins with stronger deep stratification. This is the situation between the Perth Basin (Somali Basin and Scotia Sea) and the Brazil Basin. An active overturning circulation in the Indian Ocean (and Southern Ocean [*Heywood et al.*, 2002]) does not require a large dissipation of turbulent kinetic energy, as these oceans are weakly stratified.

6. Discussion and Conclusions

[36] A year-long current meter mooring array at the southern opening of the Perth Basin, between the Broken and Naturaliste plateaus, resolved the northward and southward currents at the basin's western and eastern boundaries, respectively. In the middle of the basin weak northward transport is found. The net northward transport below $\gamma^n > 28.1$ kg m^{-3} (3200 m) into the basin is between 4.4 and 5.8 Sv. The inflowing water into the Perth Basin can be divided into two Southern Ocean origin water masses: LCDW and AABW. Net northward transport of these water masses are 2.4 to 3.3 Sv and 2.0 to 2.5 Sv, respectively. Much of the net northward transport of LCDW occurs within 1° longitude of the western boundary, while northward transport in the middle of the basin is balanced by southward flow at the eastern boundary. Northward transport of AABW occurs across much of the western part of the basin, with balancing southward and northward flow between 105.5°E and 107°E. The midbasin velocity shows significant variability and strengthening velocity toward the bottom. The northward flow of AABW ($\gamma^n > 28.2$ kg m^{-3}) must upwell within the Perth Basin as the area of this isopycnal surface is limited to the southern portion of the basin. Net upwelling of inflowing AABW results in an abyssal diapycnal velocity and diffusivity of $w^* = 2.5–3.1 \times 10^{-6}$ m s^{-1} and $\kappa = 13–15 \times 10^{-4}$ m^2 s^{-1}, respectively.

[37] Diffusivity estimates for the abyssal Perth Basin based on property conservation are several times larger than mixing estimates, using similar techniques, in the South Atlantic's Brazil Basin [*Hogg et al.*, 1982; *Morris et al.*, 2001] and Pacific Ocean [*Whitworth et al.*, 1999], and similar to mixing estimates in the Somali Basin and 3 times smaller than estimates in the Scotia Sea [*Heywood et al.*, 2002]. However, the dissipation of kinetic turbulent energy required to achieve the necessary upwelling and maintain the abyssal stratification of the Perth Basin and Scotia Sea is similar to that required in the Brazil Basin.

[38] High basin diffusivity ($>O(10^{-4}$ m^2 s^{-1})) does not necessarily imply large energy dissipation rates; the amount of energy required for mixing is dependent on the basin stratification. High diffusivity values in the Perth and Somali basins and Scotia Sea do not require unreasonable energy dissipation owing to a weakly stratified abyssal ocean. All regions of the Indian and Southern oceans are weakly stratified and therefore the meridional overturning circulation of these oceans will not require a large energy dissipation.

[39] *Wunsch and Ferrari* [2004] provide a review of vertical mixing and the potential energy sources available to the oceans to support abyssal mixing. The summary, drawn from a wide variety of published studies, is that abyssal mixing is dominated by high mixing regions surrounding complex topographic features. Ocean basin mixing estimates, as calculated in this study, provide area average mixing rates for ocean basins that include regions of complex bottom topography and smooth abyssal plains. The Perth Basin is a semi-enclosed basin with a complex bathymetric boundary and interior topographic features (Figure 1). This complex basin topography provides sites that may support elevated mixing levels at the boundary and in the interior of the basin. Indeed, enhanced vertical diffusivities are found at the boundary and within the basin interior surrounding topographic features (Figure 9).

[40] The energy to support the abyssal mixing and maintain the Perth Basin deep stratification is most likely provided by wind and tidal forcing [*Wunsch and Ferrari*, 2004]. They suggest that tidal mixing accounts for approximately half of the required abyssal mixing, with the remaining energy derived from wind forcing. Energy may also come from the generation of internal waves by the mean flow over rough topography (K. Polzin, personal communication, 2004). Wind and tidal forcing and mean flow generated internal waves ultimately supply the energy to the abyssal ocean to drive the mixing and maintain the ocean's deep stratification.

[41] The area-averaged mixing in the Perth Basin results from intense mixing at the basin boundary and in the basin interior over rough topography. The Indian Ocean is divided into numerous individual basins by complex topographic ridges (Figure 1). These topographic ridges all provide the potential to generate internal waves that ultimately provide the energy to support the Indian Ocean meridional overturning circulation. The numerous topographic features and low abyssal stratification suggest that the Indian Ocean, for a given energy dissipation, may support a larger overturning circulation than other subtropical oceans.

[42] **Acknowledgments.** B. M. S. was supported by funds from the Ocean and Climate Change Institute at the Woods Hole Oceanographic Institution, and The James S. Cole and Cecily C. Selby Endowed Fund and The Penzance Endowed Fund in support of Assistant Scientists. The mooring array was funded by Australia's CSIRO Marine Research. Comments from Trevor McDougall, John Toole, Jack Whitehead, Karen Heywood, an anonymous reviewer. and James Richman improved the manuscript. This is WHOI contribution 11374.

References

Baines, P. G., and S. Condie (1998), Observations and modelling of Antarctic downslope flows: A review, in *Ocean, Ice, and Atmosphere: Interactions at the Antarctic Continental Margin*, *Antarct. Res. Ser.*, vol. 75, edited by S. S. Jacobs and R. F. Weiss, pp. 29–49, AGU, Washington, D. C.

Barton, E. D., and A. E. Hill (1989), Abyssal flow through the Amirante Trench (western Indian Ocean), *Deep Sea Res.*, *36*, 1121–1126.

Bray, N. A., and N. P. Fofonoff (1981), Available potential energy for MODE eddies, *J. Phys. Oceanogr.*, *11*, 30–46.

Bryden, H. L., and L. M. Beal (2001), Role of the Agulhas Current in Indian Ocean circulation and associated heat and freshwater fluxes, *Deep Sea Res., Part I*, *48*, 1821–1845.

Cairns, J. L., and G. O. Williams (1976), Internal wave observations from a midwater float, *J. Geophys. Res.*, *81*, 1943–1950.

Carmack, E. C. (1977), Water characteristics of the Southern Ocean south of the Polar Front, in *Voyage of Discovery*, edited by M. Angel, pp. 15–37, Elsevier, New York.

Donohue, K. A., G. E. Hufford, and M. S. McCartney (1999), Sources and transport of the deep western boundary current east of the Kerguelen plateau, *Geophys. Res. Lett.*, *26*, 851–854.

Ferron, B., H. Mercier, K. Speer, A. Gargett, and K. Polzin (1998), Mixing in the Romanche Fracture Zone, *J. Phys. Oceanogr.*, *28*, 1929–1945.

Ganachaud, A., C. Wunsch, J. Marotzke, and J. Toole (2000), Meridional overturning and large-scale circulation of the Indian Ocean, *J. Geophys. Res.*, *105*, 26,117–26,134.

Garrett, C. J. R., and W. H. Munk (1975), Space-time scales of internal waves: A progress report, *J. Geophys. Res.*, *80*, 291–297.

Gordon, A. L., and P. Tchernia (1972), Waters of the continental margin off the Adélie Coast Antarctic, in *Antarctic Oceanology II: The Australian–New Zealand Sector*, *Antarct. Res. Ser.*, vol. 19, edited by D. E. Hayes, pp. 59–69, AGU, Washington, D. C.

Heywood, K. J., A. C. Naveira Garabato, and D. P. Stevens (2002), High mixing rates in the abyssal Southern Ocean, *Nature*, *415*, 1011–1014.

Hogg, N. G., P. Biscaye, W. Gardner, and W. J. Schmitz Jr. (1982), On the transport and modification of Antarctic Bottom Water in the Vema Channel, *J. Mar. Res.*, *40*, 231–263.

Hogg, N., G. Siedler, and W. Zenk (1999), Circulation and variability at the southern boundary of the Brazil Basin, *J. Phys. Oceanogr.*, *29*, 145–157.

Hufford, G. E., M. S. McCartney, and K. A. Donohue (1997), Northern boundary currents and adjacent recirculations off southwestern Australia, *Geophys. Res. Lett.*, *24*, 2797–2800.

Jacobs, S. (1986), Injecting ice–shelf water and air into the deep Antarctic Ocean, *Nature*, *321*, 196–197.

Kunze, E. (2003), Yes, we have no abyssal mixing, in *Near-Boundary Processes and Their Parameterization: 'Aha Hulika'a Hawaiian Winter Workshop*, edited by D. Müller and D. Henderson, pp. 85–93, Univ. of Hawaii at Manoa, Honolulu.

Macdonald, A. M. (1998), The global ocean circulation: A hydrographic estimate and regional analysis, *Prog. Oceanogr.*, *41*, 281–382.

Mantyla, A. W., and J. L. Reid (1995), On the origins of deep and bottom waters of the Indian Ocean, *J. Geophys. Res.*, *100*, 2417–2439.

Mauritzen, C., K. L. Polzin, M. S. McCartney, R. C. Millard, and D. E. West-Mack (2002), Evidence in hydrography and density fine structure for enhanced vertical mixing over the Mid-Atlantic Ridge in the western Atlantic, *J. Geophys. Res.*, *107*(C10), 3147, doi:10.1029/2001JC001114.

McCarthy, M. C., L. D. Talley, and M. O. Baringer (1997), Deep upwelling and diffusivity in the southern Central Indian Basin, *Geophys. Res. Lett.*, *24*, 2801–2804.

Morris, M. Y., M. M. Hall, L. C. St. Laurent, and N. G. Hogg (2001), Abyssal mixing in the Brazil Basin, *J. Phys. Oceanogr.*, *31*, 3331–3348.

Naveira Garabato, A. C., K. L. Polzin, B. A. King, K. J. Heywood, and M. Visbeck (2004), Widespread intense turbulent mixing in the Southern Ocean, *Science*, *303*, 210–213.

Orsi, A. H., G. C. Johnson, and J. L. Bullister (1999), Circulation, mixing, and production of Antarctic Bottom Water, *Prog. Oceanogr.*, *43*, 55–109.

Osborn, T. R. (1980), Estimates of the local rate of vertical diffusion from dissipation measurements, *J. Phys. Oceanogr.*, *10*, 83–89.

Park, Y.-H., E. Charriaud, and M. Fieux (1998), Thermohaline structure of the Antarctic Surface Water/Winter Water in the Indian sector of the Southern Ocean, *J. Mar. Syst.*, *17*, 5–23.

Polzin, K. L., J. M. Toole, J. R. Ledwell, and R. W. Schmitt (1997), Spatial variability of turbulent mixing in the abyssal ocean, *Science*, *276*, 93–96.

Rintoul, S. R. (1998), On the origin and influence of Adélie land bottom water, in *Ocean, Ice, and Atmosphere: Interactions at the Antarctic Continental Margin, Antarctic Research Series*, vol. 75, edited by S. S. Jacobs and R. F. Weiss, pp. 151–171, AGU, Washington, D. C.

Robbins, P. E., and J. M. Toole (1997), The dissolved silica budget as a constraint on the meridional overturning circulation of the Indian Ocean, *Deep Sea Res., Part I*, *44*, 879–906.

Schmitz, W. J., Jr. (1996), On the world ocean circulation: II. The Pacific and Indian oceans/A global update, *Tech. Rep. WHOI–96–08*, Woods Hole Oceanogr. Inst., Woods Hole, Mass.

Sloyan, B. M. (2005), Spatial variability of mixing in the Southern Ocean, *Geophys. Res. Lett.*, *32*, L18603, doi:10.1029/2005GL023568.

Sloyan, B. M., and S. R. Rintoul (2001), The Southern Ocean limb of the global deep overturning circulation, *J. Phys. Oceanogr.*, *31*, 143–173.

Smith, W., and D. Sandwell (1997), Global sea floor topography from satellite altimetry and ship depth soundings, *Science*, *277*, 1956–1962.

Stein, C. A., S. Stein, and A. M. Pelayo (1995), Heat flow and hydrothermal circulation, in *Seafloor Hydrothermal Systems: Physical, Chemical, Biological, and Geological Interactions*, *Geophys. Monogr. Ser.*, vol. 91, edited by S. Humphris et al., pp. 425–445, AGU, Washington, D. C.

St. Laurent, L. C., J. M. Toole, and R. W. Schmitt (2001), Buoyancy forcing by turbulence above rough topography in the abyssal Brazil Basin, *J. Phys. Oceanogr.*, *31*, 3476–3495.

Sverdrup, H. U., M. W. Johnson, and R. H. Fleming (1942), *The Oceans, Their Physics, Chemistry and General Biology*, 1087 pp., Prentice-Hall, Upper Saddle River, N. J.

Talley, L. D., and M. O. Baringer (1997), Preliminary results from WOCE hydrographic sections at 80°E and 32°S in the Central Indian Ocean, *Geophys. Res. Lett.*, *24*, 2789–2792.

Talley, L. D., J. L. Reid, and P. E. Robbins (2003), Data-based meridional overturning streamfunctions for the global ocean, *J. Clim.*, *16*, 3213–3226.

Toole, J. M., and B. A. Warren (1993), A hydrographic section across the subtropical south Indian Ocean, *Deep Sea Res.*, *40*, 1973–2019.

Warren, B. A. (1981), Deep circulation of the world ocean, in *Evolution of Physical Oceanography*, edited by B. A. Warren and C. Wunsch, pp. 6–41, MIT Press, Cambridge, Mass.

Warren, B. A. (1982), The deep water of the central Indian Basin, *J. Mar. Res.*, *40*, 823–860.

Warren, B. A., and G. C. Johnson (2002), The overflows across the Ninetyeast Ridge, *Deep Sea Res., Part II*, *49*, 1423–1439.

Whitehead, J. J. A., and L. V. Worthington (1982), The flux and mixing rates of Antarctic Bottom Water within the North Atlantic, *J. Geophys. Res.*, *87*, 7903–7924.

Whitworth, T., III (2002), Two modes of bottom water in the Australian–Antarctic Basin, *Geophys. Res. Lett.*, *29*(5), 1073, doi:10.1029/2001GL014282.

Whitworth, T., III, B. A. Warren, W. D. Nowlin Jr., S. B. Rutz, R. D. Pillsbury, and M. I. Moore (1999), On the deep western-boundary current in the southwest Pacific Basin, *Prog. Oceanogr.*, *43*, 1–54.

Wijesekera, H., L. Padman, T. Dillon, M. Levine, and C. Paulson (1993), The application of internal-wave dissipation models to a region on strong mixing, *J. Phys. Oceanogr.*, *23*, 269–286.

Wunsch, C., and R. Ferrari (2004), Vertical mixing, energy and the general circulation of the oceans, *Annu. Rev. Fluid Mech.*, *36*, 281–314, doi:10.1146/annurev.fluid.36.050802.122121.

B. M. Sloyan, CSIRO Marine and Atmospheric Research, Castray Esplanade, Hobart, TAS 7000, Australia. (bernadette.sloyan@csiro.au)